Seismic evidence for the α-β quartz transition beneath Taiwan from Vp/Vs tomography

H. Kuo-Chen,[1,2,3] F. T. Wu,[1,3] D. M. Jenkins,[1] J. Mechie,[4] S. W. Roecker,[5] C.-Y. Wang,[2] and B.-S. Huang[6]

Received 22 August 2012; revised 16 October 2012; accepted 18 October 2012; published 20 November 2012.

[1] Knowledge of the rock types and pressure-temperature conditions at crustal depths in an active orogeny is key to understanding the mechanism of mountain building and its associated modern deformation, erosion and earthquakes. Seismic-wave velocities by themselves generally do not have the sensitivity to discriminate one rock type from another or to decipher the P-T conditions at which they exist. But laboratory-measured ratios of velocities of P to S waves (Vp/Vs) have been shown to be effective. Results of 3-D Vp and Vp/Vs tomographic imaging based on dense seismic arrays in the highly seismic environment of Taiwan provides the first detailed Vp/Vs structures of the orogen. The sharp reduction in the observed Vp/Vs ratio in the felsic core of the mountain belts implies that the α-β quartz transition temperature is reached at a mean depth of 24 $\pm$ 3 km. The transition temperature is estimated to be 750 $\pm$ 25°C at this depth, yielding an average thermal gradient of 30 $\pm$ 3°C/km.
Citation: Kuo-Chen, H., F. T. Wu, D. M. Jenkins, J. Mechie, S. W. Roecker, C.-Y. Wang, and B.-S. Huang (2012), Seismic evidence for the α-β quartz transition beneath Taiwan from Vp/Vs tomography, *Geophys. Res. Lett.*, *39*, L22302, doi:10.1029/2012GL053649.

1. Introduction

[2] One of the goals of seismic imaging is to infer the nature of the material through which the waves propagate, providing in effect a subsurface geological map. Vp or Vs alone is insufficient for separating the gross rock compositions from the pressure and temperature effects, but laboratory measurements show that the Vp/Vs ratios are sensitive to them [*Kern*, 1982]. Although the ratios are noticeably pressure-dependent below 200 MPa (~7 km depth) due to the presence of micro-cracks, above 200 MPa these cracks close and the Vp/Vs ratios correlate with modal mineralogical composition and do not significantly change with pressure [*Wang and Ji*, 2009]. Thus, the seismic velocity ratios can be interpreted in terms of crustal rock materials [*Hyndman*, 1979; *Castagna et al.*, 1985; *Jizba*, 1991; *Holbrook et al.*, 1992; *Castagna et al.*, 1993; *Christensen*, 1996; *Matsumoto et al.*, 2010]. Vp/Vs ratios for crack-free rocks vary in the range of 1.5–1.9, with quartz-rich rocks generally in the lower and mafic rocks in the higher ranges [*Kern*, 1982; *Christensen*, 1996]. In a global survey, *Zandt and Ammon* [1995] argued for the wide presence of felsic rocks in Mesozoic-Cenozoic active orogenic belts based on observed low Vp/Vs ratios. Low ratios have also been obtained for the American Cordillera [*Lowry and Pérez-Gussinyé*, 2011], Qaidam [*Jiang et al.*, 2006], Pamir [*Mechie et al.*, 2012], and Tibet [*Mechie et al.*, 2004].

[3] Laboratory measurements show a further property of Vp/Vs ratios in quartz-bearing rocks: as temperature rises, a minimum is reached at the α-β quartz transition (ABQT) and beyond the transition the ratio rises sharply [*Kern*, 1982; *Shen et al.*, 1993; *Ohno et al.*, 2006]. Low Vp/Vs ratios that would imply the presence of ABQT have not appeared in global surveys, probably because of the averaging effects in sampling large bodies and limited resolution. However, *Mechie et al.* [2004] have determined ratios as low as ~1.63 in central and southern Tibet using 2-D seismic arrays and found low ratios at depths of 18 and 32 km, respectively, and estimated the corresponding temperatures at ~700 and ~800°C from the known phase diagram of the α-β quartz transition (ABQT) [*Shen et al.*, 1993]. An exceptional opportunity arose for measuring the Vp/Vs ratio in Taiwan, an active orogeny using data from the TAIGER (Taiwan Integrated Geodynamic Research) project of 2004–2009 [*Kuo-Chen et al.*, 2012]. A large amount of seismic data was acquired because of the very high local seismicity and the dense arrays used to record it (Figure 1), rendering it possible for the high-resolution imaging of 3-D Vp and Vp/Vs structures. An independent estimate of temperature inside an active orogen based on ABQT may provide important constraints for modeling geological processes in progress.

2. Tectonic Setting

[4] The young and active Taiwan orogen (~6.5 Ma) [*Chai*, 1972] is a result of the collision of the oceanic Philippine Sea plate with the eastern edge of the Eurasian plate, with the latter including a part of the Eurasian continental shelf and the South China Sea basin (Figure 1). In the main collision zone, the principal geologic/tectonic units at the surface are defined from east to west as follows: (1) the Coastal Range (CoR), which is the compressed ancient Luzon Arc and its forearc; (2) the Longitudinal Valley Fault (LVF), which is the suture between the Eurasian and Philippine Sea plates that separates the CoR from the Central Range; (3) the Central Range (CR), composed of the pre-Tertiary basement of the continental margin of the Eastern Central Range (ECR) and the Miocene to Eocene slates of the Western Central Range

[1]Department of Geological and Environmental Sciences, State University of New York at Binghamton, Binghamton, New York, USA.
[2]Institute of Geophysics, National Central University, Jhongli, Taiwan.
[3]Department of Earth Sciences, University of Southern California, Los Angeles, California, USA.
[4]Deutsches GeoForschungsZentrum, Potsdam, Germany.
[5]Department of Earth and Environmental Sciences, Rensselaer Polytechnic Institute, Troy, New York, USA.
[6]Institute of Earth Sciences, Academia Sinica, Taipei, Taiwan.

Corresponding author: H. Kuo-Chen, Institute of Geophysics, National Central University, Jhongli 32054, Taiwan. (kuochen@ncu.edu.tw)

0094-8276/12/2012GL053649

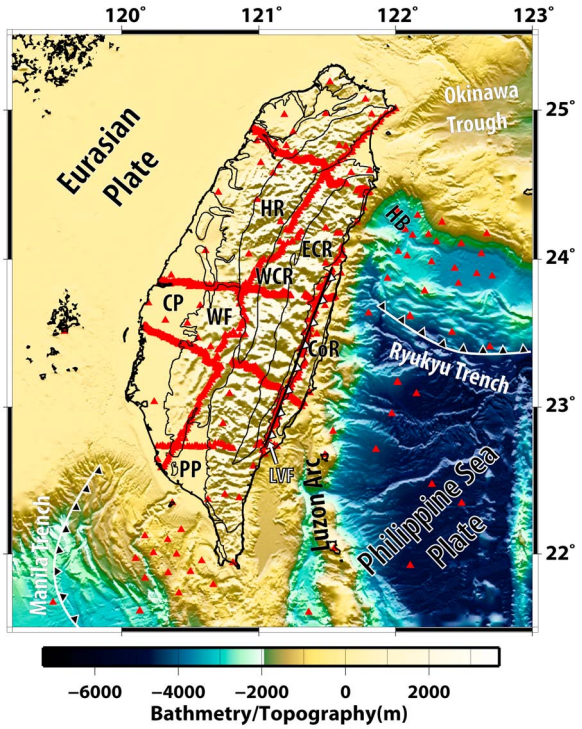

Figure 1. Tectonic setting and seismic stations. Red triangles: seismic stations. Abbreviations: CP: Coastal Plain; WF: Western Foothills; HR: Hsuehshan Range; WCR: Western Central Range; ECR: Eastern Central Range; CoR: Coastal Range; PP: Pingtung Plain; HB: Hoping Basin; LVF: Longitudinal Valley Fault.

(WCR); (4) the Hsuehshan Range (HR), which is built mostly from Eocene and Oligocene continental shelf sediments from the west; (5) the Western Foothills (WF), composed of accreted and deformed sediments in the foreland basin; and (6) the Coastal Plain (CP), which is the present-day foreland basin (Figure 1) [*Ho*, 1986]. The Central Range has attained high topography (~3000 m) and has a modern uplift rate approaching 20 mm/yr [*Ching et al.*, 2011]. The intense deformation that has occurred over the past 6.5 Ma has led to the formation of a significantly thickened crustal root (~50 km) beneath the Central Range based on tomographic studies [e.g., *Kuo-Chen et al.*, 2012].

3. Data

[5] With the aim of producing high-resolution seismic imaging of the Taiwan orogen, we merged the dataset of the TAIGER project, comprising approximately 2,800 temporary seismic stations on and around Taiwan, with the data of the permanent seismic networks on land (Figure 1) [*Kuo-Chen et al.*, 2012]. The data from ocean bottom seismometers and dense seismic arrays along transects (4 EW and 2 NS) improved the spatial resolution of tomographic images. For S waves we picked SH arrivals on the tangential components to minimize the problem of SV/P interference (Figure S1 in Text S1 in the auxiliary material).[1] Moreover, the coherent P and S arrival picks from strategically located small events recorded at the full dense arrays could be used for verifying the key features in the Vp and Vp/Vs images (Figures S1 and S4 in Text S1). In this study, the Vp and Vp/Vs models are constructed with 6 × 6 × 6 km grids and ~3,000 sources are used for the tomographic inversions. Based on checkerboard tests, the structural images down to 60 km for Vp/Vs and to a greater depth for Vp are reasonably well resolved - the difference arises from the better spatial coverage of ray paths of P waves than that of S waves (Figures S2 and S3 in Text S1; see detailed descriptions of methods and resolution tests in the auxiliary material).

[1]Auxiliary materials are available in the HTML. doi:10.1029/2012GL053649.

4. Low Vp/Vs Ratios Beneath the Central Range

[6] With frequent local earthquakes under Taiwan a large number of SH arrivals picks were obtained from the TAIGER seismograms. Combining with the P picks used in *Kuo-Chen et al.* [2012] and employing the same Roecker algorithm [*Roecker et al.*, 2006] we jointly invert the P and S picks to derive 3D Vp and Vp/Vs models. As demonstrated by *Menke* [2005] such inversion resolves better the resulting models than inverting for Vp and Vs independently. The 0–6 km slice in Figure 2a shows that Vp/Vs variations are closely correlated with changes in surface geology similar to Vp [*Kuo-Chen et al.*, 2012]; regions of low Vp (3.5 to 5.0 km/s) [*Kuo-Chen et al.*, 2012] and low Vp/Vs (<1.73) coincide with the major sedimentary basins in Taiwan (Figures 1 and 2a). Low Vp/Vs values are also associated with the deep (>12 km) basins such as the Pingtung Plain (PP) and the Hoping Basin (HB) offshore (Figures 1 and 2a). At greater crustal depths beneath the Central Range, at the depth between 12 and 42 km, a zone of remarkably low Vp/Vs ratios of less than 1.7 is found (Figures 2c and 2d). With the earthquakes at lower crustal depths the seismic rays traveling to the eastern and western stations traverse through regions of relatively high ratios and only the waves reaching the stations in the high ranges sample the low ratio materials (Figure 2c). In Figure 2d, the Ts/Tp ratios for stations on both the east and west sides of the Central Range are greater than 1.73 but for stations in the high ranges the values are less than 1.73. The predicted arrival times of P and S waves using our Vp and Vp/Vs models superposed on the seismogram plots show good agreement and the residuals are general smaller than 0.3 sec (Figure S4 in Text S1).

[7] To facilitate interpretation, we compiled Vp/Vs vs Vp for a host of rocks as shown in Figure 3a, based on published laboratory results [*Hyndman*, 1979; *Castagna et al.*, 1985; *Jizba*, 1991; *Holbrook et al.*, 1992; *Castagna et al.*, 1993; *Christensen*, 1996; *Matsumoto et al.*, 2010]. The mafic rocks (blue circles) are generally in the upper right part of the diagram and the felsic rocks (red circles) appearing in the middle, hover around 1.73 or less than 1.6, for quartzite and quartzite granulite. In the lower left are rocks that belong to the quartz-rich sandstone and mudrock, materials that are found in the western Taiwan basins above 12 km. Based on the Vp/Vs ratios in Figure 3a, we infer from the tomographic image (Figure 2b) the existence of a felsic core in the mid-crust under the Central Range, surrounded by materials with higher ratios (Figures 2b and 2c). This inference is consistent with the abundance of granitic rocks in the eastern Central Range [*Lan et al.*, 1996, 2002]. The extensive felsic core of the Central Range as implied by the Vp/Vs resides in the area

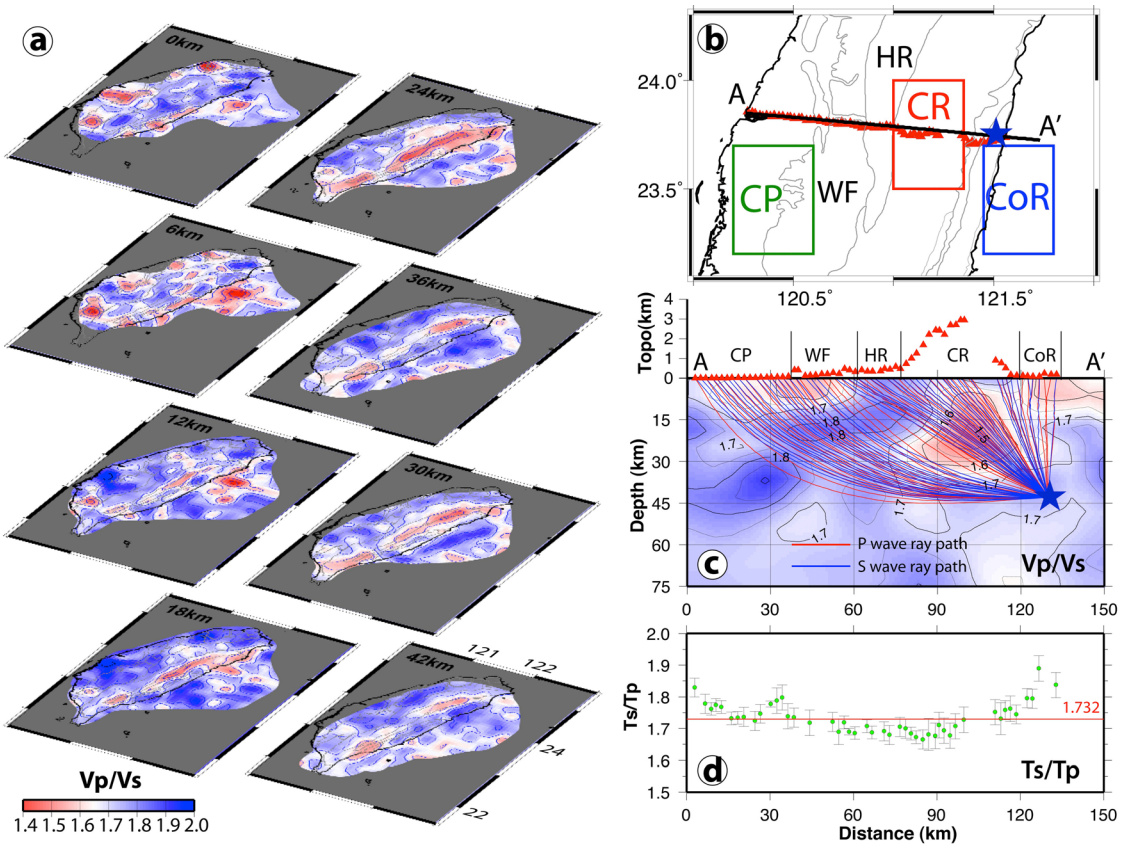

Figure 2. (a) Horizontal slices through the 3D tomographic model showing Vp/Vs ratios. (b) Map view of selected regions for Vp-Vp/Vs-depth profiles in Figures 3b and 3c. Red triangles: seismic stations. Blue star: epicenter of earthquake for Figures 2c and 2d. (c) The depth profile of Vp/Vs tomography (Figure 2b for map view) with the raypaths of P (blue lines) and S waves (red lines). The low Vp/Vs structure is resolvable with seismic stations across the mountain belts (CR and HR). (d) Ts/Tp (apparent Vp/Vs) along the EW seismic array. Bars: pick uncertainties. (See Figure 2b for locations of the seismic array and earthquake).

where apparent collision thickening is at its maximum [*Kuo-Chen et al.*, 2012].

5. The α-β Quartz Transition (ABQT) and P/T Beneath the Central Range?

[8] To explore further the possible significance of our Vp/Vs observations we choose three vertical profiles along a cross section that includes (a) the Coastal Plain of western Taiwan, (b) the Central Range and (c) the Coastal Range (Figures 2b, 3b, and 3c). The average values of Vp/Vs are plotted. While the values for (a) and (c) are generally higher than 1.73, in (b), they are noticeably lower than 1.73 in the depth range of 12–30 km and a minimum of 1.55 is reached at ~24 km. In Figure 3b, it is obvious that the low Vp/Vs values occur in a depth range of low Vp.

[9] The systematic decrease and increase of Vp/Vs in the mid-crust under the Central Range is quite clear and significant. In exploring the factors that may affect Vp/Vs we rule out fluid pressure or melting (see discussion), but it is well known that a single-crystal quartz undergoes a phase transition at 575°C under atmospheric pressure from the lower-symmetry trigonal form, α-quartz, to the higher-symmetry hexagonal form, β-quartz [*Ohno et al.*, 2006]. This transition temperature (*Ttr*) rises with pressure at a well-established rate of 0.256°C/MPa [*Shen et al.*, 1993]. As temperature approaches *Ttr*, α-quartz undergoes elastic softening due to the volume differential between the two forms, which decreases Vp more than Vs causing a marked decrease in the Vp/Vs ratio [*Kern*, 1982]. A minimum of ~1.6 or less is reached when this transition occurs [*Kern*, 1982]. The ratio increases as the temperature increases beyond *Ttr*. This transition has been observed not only in experiments on a single quartz crystal at atmospheric pressure [*Ohno et al.*, 2006] but also on quartz-bearing rocks at high pressures [*Kern*, 1982]. Figure 4b shows the Vp/Vs of a single quartz crystal, several felsic rocks, and our Central Range profile. In this figure, our Central Range profile is next to the curve for a rock with 22% quartz content [*Kern*, 1982]. The implied quartz content of the low Vp/Vs materials is reasonable in view of *Lan et al.* [1996] estimate of 14–43% quartz content for the granitic rocks in the Central Range. Assuming the minimum in our profile represents the ABQT at ~24 ± 3 km (~686 MPa) and applying *Shen et al.* [1993] relation we arrive at a *Ttr* of about 750 ± 25°C (error from a half of a grid cell in the model). We note that the 1D profile we obtain is not as sharp as the laboratory ABQT curves. The more gradual variation in our curve may come from averaging the values in the sampling box under the Central Range, as well as the effect of sampling

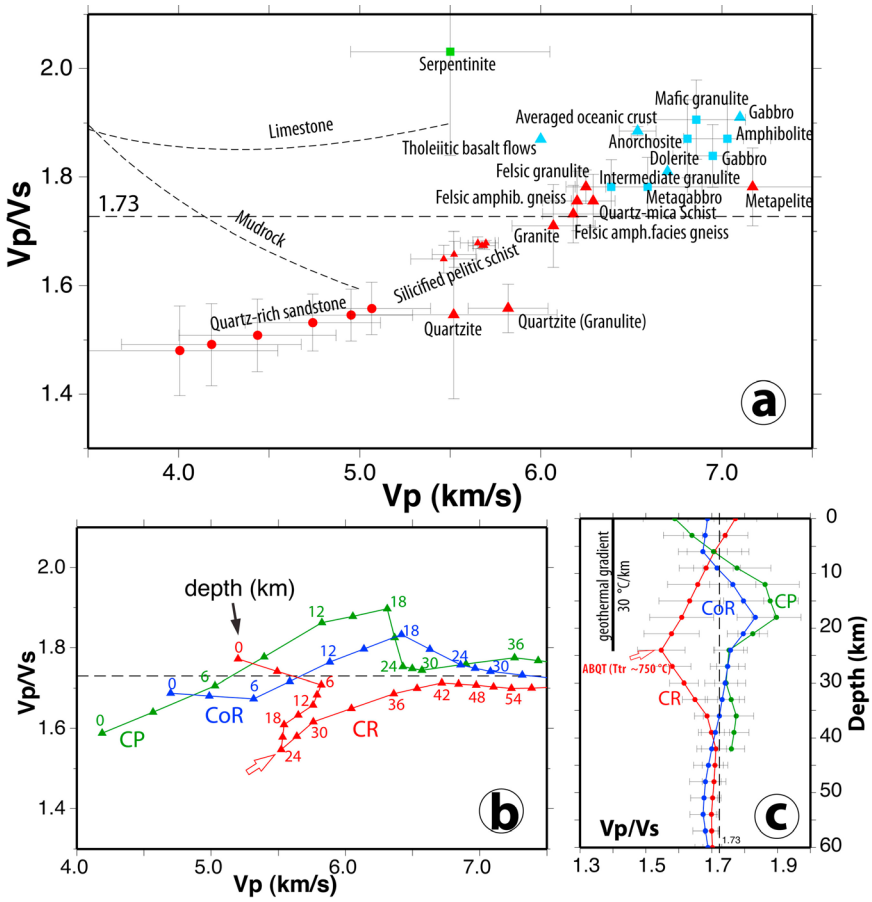

Figure 3. (a) P-velocity (Vp) versus Vp/Vs ratio for crustal rocks [*Hyndman*, 1979; *Castagna et al.*, 1985; *Jizba*, 1991; *Holbrook et al.*, 1992; *Castagna et al.*, 1993; *Christensen*, 1996; *Matsumoto et al.*, 2010]. Error bar: 1 σ. Dashed lines: regression lines for different rocks [*Castagna et al.*, 1985, 1993]. Red color-coded symbols: felsic rocks. Blue color-coded symbols: mafic rocks. Green color-coded symbol: hydrated rock. (b) Vp-Vp/Vs-depth profiles for different tectonic environments. Number: depth (km). Red arrow: Lowest Vp (5.52 $\pm$ 0.31 km/s) and Vp/Vs (1.55 $\pm$ 0.07) ratio occurring at 24 km depth in the Central Range. (c) Vp/Vs versus depth profiles for different tectonic environments. Error bar: 1 σ.

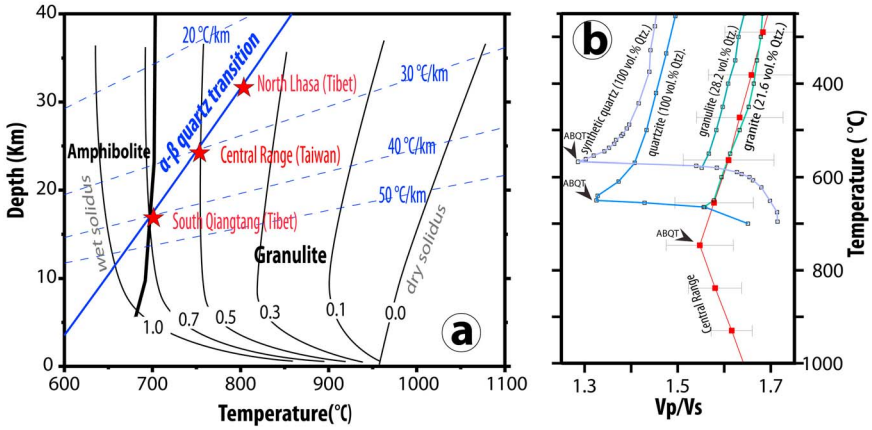

Figure 4. (a) Temperature-pressure diagram for metamorphic facies, solidus curves, and thermal gradients. Red star: the depth of the α-β quartz transition found in Tibet [*Mechie et al.*, 2004] and Taiwan (this study). Blue dotted line: thermal gradient. Thin black line: Solidus curve for given H_2O activity [*Ebadi and Johannes*, 1991]. Thick black line: boundary of metamorphic facies. (b) Vp/Vs versus temperature profiles from rock experiments with different confining pressures [*Kern*, 1982; *Ohno et al.*, 2006]. Red line: Vp/Vs versus temperature profile in the Central Range. 30°C/km is the thermal gradient obtained in this study after conversion from the ABQT depth to temperature. Qtz.: quartz. Error bar: 1 σ of Vp/Vs ratio.

in a volume of rock with material and thermal heterogeneity due to complex deformation.

[10] Using this transition as a thermometer we obtain a present-day geothermal gradient of about 30 $\pm$ 3°C/km above a depth of 24 $\pm$ 3 km in the Central Range (Figure 4a). Such a value is consistent with an estimate of 350°C at ~12 km to explain the cutoff depth of seismicity [*Wu et al.*, 1997; *Lin*, 2000] and 680–750°C at 20 $\pm$ 5 km depth to account for low Qp (287.7 $\pm$ 2.1) and Qs (219.0 $\pm$ 1.5) [*Lee et al.*, 2010]. Compared to a temperature of 500°C from Raman spectroscopy of carbonaceous materials (RSCM) in the eastern Central Range [*Beyssac et al.*, 2007], our estimate is significantly higher, but the RSCM temperature estimate is not associated with a definite depth and represents conditions inside the orogen before the exhumation. The rapid exhumation (10–20 mm/yr) of the Central Range [*Lee et al.*, 2006; *Ching et al.*, 2011] could have led to an uplift of the isotherms under the high ranges, raising the temperature at shallower depth and creating a horizontal temperature gradient; the contrast of Vp and Vp/Vs at the middle- to lower-crustal levels with those of the surrounding areas.

6. Discussion and Conclusions

[11] The α- β quartz transition from Vp/Vs imaging could be a powerful indicator for the P/T conditions in the crust. However, it depends on the availability of dense seismic stations and availability of seismic sources. Also, there are other factors than P/T to take into consideration: crustal anisotropy and water content among them. Although the metamorphic rocks of Taiwan are highly anisotropic, as high as 15% (N. Christensen, personal communication, 2009), studies of local shear wave splitting measurements in the Central Range have obtained δt of 0 to 0.3 sec, but mostly less than 0.1 sec for paths mostly in the Central Range [*Chang et al.*, 2009]. These δt's correspond to 0–6% anisotropy in the upper 30 km of the crust. They are equal to or less than the travel time residuals of the tomographic inversion results. Hence, the assumption of isotropy is a good approximation to the rock properties to a first order. The fluid pressure or bounded water can affect Vp/Vs noticeably. In general, structurally-bound water yields high Vp/Vs ratios (see, e.g., data for serpentinite in Figure 3a) and high fluid pressure and partial melting also lead to higher Vp/Vs ratio [*Mueller and Massonne*, 2001]. Regarding the fluid or partial melting, the magnetotelluric transect across the Central Range in the vicinity of our 1D profiles shows a resistivity of ~500 Ohm-m in the low Vp/Vs zone, signifying anhydrous conditions [*Bertrand et al.*, 2009]. As shown in Figure 4a, rocks with H_2O activity below 0.5 should remain solid [*Ebadi and Johannes*, 1991; *Brown*, 2001]. Thus, it is the combination of being dry and under elevated temperature from rapid exhumation in the middle and lower crust under the Central Range that allowed the ABQT to occur.

[12] In a young orogen such as Taiwan where an extensive root system is extant [*Wu et al.*, 1997; *Kuo-Chen et al.*, 2012] and rapid deformation and uplifting are well-documented [*Hsu et al.*, 2009; *Ching et al.*, 2011], the knowledge of the present P/T conditions and materials in the core of the orogen could help in the understanding of the dynamics of mountain building. *Lowry and Pérez-Gussinyé* [2011] recently proposed that the presence of abundant quartz in the continental crust is important in localizing deformation; while they deem hydration weakening as one of the conditions in the feedback processes the ABQT in Taiwan may play the role [*Mechie et al.*, 2004]. In any case, Taiwan is an excellent site where patterns of strain focusing and crustal weakening during the early stages of tectonic deformation can be explored in detail.

[13] **Acknowledgments.** The TAIGER project was supported by the Continental Dynamics Program of the National Science Foundation (EAR0410227 and EAR1010645). H. K-C was also supported by National Science Council of Taiwan. Discussions with C.Y. Lan, D. Okaya, N. Christensen, R. P. Wintsch, J.-C. Sibuet, and E.-C. Yeh are very helpful. Comments by V. Schulte-Pelkum, B. Schmandt, A. Jones, and one anonymous reviewer are highly appreciated.

[14] The Editor thanks Brandon Schmandt and an anonymous reviewer for their assistance in evaluating this paper.

References

Bertrand, E., M. Unsworth, C.-W. Chiang, C.-S. Chen, C.-C. Chen, F. Wu, E. Trkoğlu, H.-L. Hsu, and G. Hill (2009), Magnetotelluric evidence for thick-skinned tectonics in central Taiwan, *Geology*, *37*, 711–714, doi:10.1130/G25755A.1.

Beyssac, O., M. Simoes, J. P. Avouac, K. A. Farley, Y.-G. Chen, Y.-C. Chan, and B. Goffé (2007), Late Cenozoic metamorphic evolution and exhumation of Taiwan, *Tectonics*, *26*, TC6001, doi:10.1029/2006TC002064.

Brown, M. (2001), Crustal melting and granite magmatism: key issues, *Phys. Chem. Earth*, *26*, 201–212, doi:10.1016/S1464-1895(01)00047-3.

Castagna, J. P., M. L. Batzle, and R. L. Eastwood (1985), Relationships between compressional-wave and shear-wave velocities in clastic silicate rocks, *Geophysics*, *50*, 571–581, doi:10.1190/1.1441933.

Castagna, J. P., M. L. Batzle, and T. K. Kan (1993), Rock physics: The link between rock properties and AVO response, in *Offset-Dependent Reflectivity: Theory and Practice of AVO Analysis*, *Invest. Geophys. Ser.*, vol. 8, edited by J. P. Castagna and M. M. Backus, pp. 135–171, Soc. of Explor. Geophys., Tulsa, Okla., doi:10.1190/1.9781560802624.

Chai, B. H. T. (1972), Structure and tectonic evolution of Taiwan, *Am. J. Sci.*, *272*, 389–422, doi:10.2475/ajs.272.5.389.

Chang, E. T. Y., W. T. Liang, and Y. B. Tsai (2009), Seismic shear-wave splitting in upper crust characterized by Taiwan tectonic convergence, *Geophys. J. Int.*, *177*, 1256–1264, doi:10.1111/j.1365-246X.2009.04110.x.

Ching, K.-E., M.-L. Hsieh, K. M. Johnson, K.-H. Chen, R.-J. Rau, and M. Yang (2011), Modern vertical deformation rates and mountain building in Taiwan from precise leveling and continuous GPS observations, 2000–2008, *J. Geophys. Res.*, *116*, B08406, doi:10.1029/2011JB008242.

Christensen, N. I. (1996), Poisson's ratio and crustal seismology, *J. Geophys. Res.*, *101*, 3139–3156, doi:10.1029/95JB03446.

Ebadi, A., and W. Johannes (1991), Beginning of melting and composition of first melts in the system Qz-Ab-Or-H_2O-CO_2, *Contrib. Mineral. Petrol.*, *106*, 286–295, doi:10.1007/BF00324558.

Ho, C. S. (1986), *An Introduction to the geology of Taiwan: explanatory text of the geologic map of Taiwan*, p. 163, Central Geological Survey, Taiwan.

Holbrook, W. S., W. D. Mooney, and N. I. Christensen (1992), The seismic velocity structure of the deep continental crust, in *Continental Lower Crust*, edited by D. M. Fountain, R. Arculus, and R. W. Kay, pp. 1–43, Elsevier, Amsterdam.

Hsu, Y.-J., S.-B. Yu, M. Simons, L.-C. Kuo, and H.-Y. Chen (2009), Interseismic crustal deformation in the Taiwan plate boundary zone revealed by GPS observations, seismicity, and earthquake focal mechanisms, *Tectonophysics*, *479*, 4–18, doi:10.1016/j.tecto.2008.11.016.

Hyndman, R. D. (1979), Poisson's ratio in the oceanic crust—A review, *Tectonophysics*, *59*, 321–333, doi:10.1016/0040-1951(79)90053-2.

Jiang, M., A. Galvé, A. Hirn, B. de Voogd, M. Laigle, H. P. Su, J. Diaz, J. C. Lépine, and Y. X. Wang (2006), Crustal thickening and variations in architecture from the Qaidam basin to the Qang Tang (north-central Tibetan Plateau) from wide-angle reflection seismology, *Tectonophysics*, *412*, 121–140, doi:10.1016/j.tecto.2005.09.011.

Jizba, D. L. (1991), Mechanical and acoustical properties of sandstones and shales, PhD dissertation, 260 pp., Stanford Univ., Stanford, Calif.

Kern, H. (1982), Elastic-wave velocity in crustal and mantle rocks at high pressure and temperature: The role of the high-low quartz transition and of dehydration reactions, *Phys. Earth Planet. Inter.*, *29*, 12–23, doi:10.1016/0031-9201(82)90133-9.

Kuo-Chen, H., F. T. Wu, and S. W. Roecker (2012), Three-dimensional P velocity structures of the lithosphere beneath Taiwan from the analysis of TAIGER and related seismic datasets, *J. Geophys. Res.*, *117*, B06306, doi:10.1029/2011JB009108.

Lan, C.-Y., B.-M. Jahn, S. A. Mertzman, and T.-W. Wu (1996), Subduction-related granitic rocks of Taiwan, *J. Southeast Asian Earth Sci.*, *14*, 11–28, doi:10.1016/S0743-9547(96)00017-7.

Lan, C.-Y., C.-S. Lee, J. J.-S. Chen, C.-Y. Lu, S. A. Mertzman, and T.-W. Wu (2002), Nd-Sr isotopic composition and geochemistry of sediments from Taiwan and their implications, *West. Pac. Earth Sci.*, *2*, 205–222.

Lee, Y.-H., C.-C. Chen, T.-K. Liu, H.-C. Ho, H.-Y. Lu, and W. Lo (2006), Mountain building mechanisms in the southern Central Range of the Taiwan Orogenic Belt—From accretionary wedge deformation to arc-continental collision, *Earth Planet. Sci. Lett.*, *252*, 413–422, doi:10.1016/j.epsl.2006.09.047.

Lee, C.-P., N. Hirata, B.-S. Huang, W.-G. Huang, and Y.-B. Tsai (2010), Evidence of a highly attenuative aseismic zone in the active collision orogen of Taiwan, *Tectonophysics*, *489*, 128–138, doi:10.1016/j.tecto.2010.04.009.

Lin, C.-H. (2000), Thermal modeling of continental subduction and exhumation constrained by heat flow and seismicity in Taiwan, *Tectonophysics*, *324*, 189–201, doi:10.1016/S0040-1951(00)00117-7.

Lowry, A. R., and M. Pérez-Gussinyé (2011), The role of crustal quartz in controlling Cordilleran deformation, *Nature*, *471*, 353–357, doi:10.1038/nature09912.

Matsumoto, Y., M. Ishikawa, M. Terabayashi, and M. Arima (2010), Simultaneous measurements of compressional wave and shear wave velocities, Poisson's ratio, and Vp/Vs under deep crustal pressure and temperature conditions: Example of silicified politic schist from Ryoke belt, Southwest Japan, *Isl. Arc*, *19*, 30–39, doi:10.1111/j.1440-1738.2009.00695.x.

Mechie, J., S. V. Sobolev, L. Ratschbacher, A. Y. Babeyko, G. Bock, A. G. Jones, K. D. Nelson, K. D. Solon, L. D. Brown, and W. Zhao (2004), Precise temperature estimation in the Tibetan crust from seismic detection of the α-β quartz transition, *Geology*, *32*, 601–604, doi:10.1130/G20367.1.

Mechie, J., et al. (2012), Crustal and uppermost mantle velocity structure along a profile across the Pamir and southern Tien Shan as derived from project TIPAGE wide-angle seismic data, *Geophys. J. Int.*, *188*, 385–407, doi:10.1111/j.1365-246X.2011.05278.x.

Menke, W. (2005), Case studies of seismic tomography and earthquake location in a regional context, in *Seismic Earth: Array Analysis of Broadband Seismograms*, *Geophys. Monogr. Ser.*, vol. 157, edited by A. Levander and G. Nolet, pp. 7–36, AGU, Washington, D. C., doi:10.1029/157GM02.

Mueller, H. J., and H.-J. Massonne (2001), Experimental high pressure investigation of partial melting in natural rocks and their influence on V_p and V_s, *Phys. Chem. Earth, Part A*, *26*, 325–332, doi:10.1016/S1464-1895(01)00062-X.

Ohno, I., K. Harada, and C. Yoshitomi (2006), Temperature variation of elastic constants of quartz across the α-β transition, *Phys. Chem. Miner.*, *33*, 1–9, doi:10.1007/s00269-005-0008-3.

Roecker, S., C. Thurber, and K. Roberts (2006), Refining the image of the San Andreas Fault near Parkfield, California using a finite difference travel time computation technique, *Tectonophysics*, *426*, 189–205, doi:10.1016/j.tecto.2006.02.026.

Shen, A. H., W. A. Bassett, and I.-M. Chou (1993), The α-β quartz transition at high temperatures and pressures in a diamond-anvil cell by laser interferometry, *Am. Mineral.*, *78*, 694–698.

Wang, Q., and S. Ji (2009), Poisson's ratios of crystalline rocks as a function of hydrostatic confining pressure, *J. Geophys. Res.*, *114*, B09202, doi:10.1029/2008JB006167.

Wu, F., R. J. Rau, and D. Salzberg (1997), Taiwan orogeny: thin-skinned or lithospheric collision?, *Tectonophysics*, *274*, 191–220, doi:10.1016/S0040-1951(96)00304-6.

Zandt, G., and C. J. Ammon (1995), Continental crust composition constrained by measurements of crustal Poisson's ratio, *Nature*, *374*, 152–154, doi:10.1038/374152a0.